AUTONOMOUS VISION-BASED DEEP SPACE NAVIGATION WITH A MULTI-CAMERA SYSTEM: OVERVIEW, SCENARIOS AND HARDWARE AND SOFTWARE DESIGN

Hormigo T.(1), Santos A.(1), Mano C.(1), Pinheiro P.(1), Posse C.(1), Oliveira J.(1), Câmara F.(1) *(1)*
Spin.Works SA, Rua de Fundões n.º151, 3700-121 São João da Madeira, Portugal,
(+351)256 001 949, info@spinworks.pt

ABSTRACT

A significant change is currently occurring in the near-Earth space sector with the introduction of large constellations, propelled by the increasing use of COTS systems, small-scale industrialization of space parts production and the strong reduction in the cost of access to space.

Although the first steps towards the outward expansion of this movement into deep space have already taken place (including the MarCO [1] and LICIA [2], which were made part of the NASA's Insight and DART missions, respectively), and many of the upcoming planetary and small body missions are considering the inclusion of small rideshare missions (the 10 cubesats on board the NASA Artemis I mission to Lunar orbit, as well as the ASPECT [3] and Juventas [4] cubesats riding with ESA's Hera mission), the need for automation is a pre-condition to their future generalization, given the operations costs associated to each individual mission, especially when critical manoeuvres are concerned (approach, orbit insertion, deorbit, descent and landing phases as well as during aerobraking campaigns). Critically, the complexity of a given mission does not automatically scale with the spacecraft size; operations costs can therefore be expected to limit any potential savings in future missions unless automation is considered from the early stages of mission design and development.

One key element to automation is navigation, with computer vision seen as a highly promising source of precise measurements to help guide a spacecraft in the latter stages of flights toward a designated target. The advantages of this approach include power consumption (given the use of passive sensors), relatively low cost and the multiple use of cameras (for navigation, engineering and potentially scientific data observations, although effectively combining all three often proves impossible). The main disadvantages, on the other hand, are also well known (scale ambiguity, the need to carry along significant processing power able to perform data reduction in real-time, and the high reliability and performance requirements commonly associated to deep space missions). With the recent insertion of space-certified high performance COTS components, however, it would appear that the time is right to investigate compact, light, low-cost and integrated solutions potentially enabling entirely automated missions - from launcher separation until arrival. As such, we hereby describe the proposed development of a miniaturized (4U) multi-camera vision-based navigation system for small & autonomous deep space missions, an R&D project targeting TRL 5 while setting the stage for concurrent projects to reach TRL 9 in the near to mid-term future.

In this work we establish the overall system design as well as its' hardware and software architecture (which can also be complemented with other sensors such as an IMU and a radar or Lidar altimeter), including both its sensing, processing and structural/acommodation elements. In addition, we provide a brief overview of two pertinent scenarios – a small body mission and a commercial lunar landing mission, for which we have developed a suitable measurement strategy and techniques adopted for each phase, taking into account a set of assumptions and the expected performance given the high-level system specifications.

Finally, we present in more detail each of the key system components: two star trackers (0.5U each), a high-resolution camera (2U), and a high performance processing board (<1U) along with the on board image processing library.

1 INTRODUCTION

The IONEA (Instrument for Optical Navigation and Autonomous Exploration) project is an R&D contract to develop a prototype system concept aiming at full rigid-body state determination (attitude and position) throughout a deep space mission using vision, and is built on the observation that during a large fraction of any given mission only a limited positioning accuracy is required to arrive at the intended target, with the need for additional trajectory refinement growing only by the final weeks and days prior to arrival at the targeted body.

While the main innovation with respect to existing systems is the use of a vision-only approach to position estimation, the approach to attitude estimation is fully established: most deep space missions use two star trackers for that purpose, which at the present time are already highly miniaturized components such as to fit almost any volume even for relatively high precision [5]. On the other hand, if precise position estimation is also sought in addition to attitude estimation there is an additional trade off to be made, since miniaturized star trackers can trade some accuracy and sensitivity for a wider field-of-view as long as at least 3 bright stars can always be detected, while if high accuracy is specifically required then either a higher pixel count is needed (with the associated size and power consumption) or the field-of-view needs to be narrower (in which case higher sensitivity will be mandatory to ensure full sky coverage), or a combination of the two. In the present work we have added a narrow angle camera in addition to the two star trackers in order to provide high accuracy optical navigation measurements. For this purpose, we specifically avoided designing a camera exclusively for optical navigation purposes, and instead adapted an existing panchromatic camera from a multispectral imager developed for a prior Earth Observation research project, in order to assess whether a camera originally developed for Earth Observation (and which could ultimately be used for mapping purposes upon arrival at a deep space target) could also be suited for autonomous deep space navigation.

Finally, and in order to acquire and process the incoming visual data with the goal of extracting useful navigation observations from all three cameras, we developed a general-purpose data processor (derived from a miniaturized payload data processor which we use for other terrestrial applications) which includes a multi-core processor and an FPGA. Configuration and control software along with suitable IP cores have been developed to operate each of the three devices. An image processing library has also been established that implements hardware-accelerated algorithms to extract meaningful information from visual images for a number of relevant applications; this is detailed in section 2.2. As a first approach, the 3 cameras and the processing unit are installed in a structure measuring 20 x 20 x 10 cm (4U), which is both small enough to fit on nearly any real mission and large enough to allow placing the two star trackers in a wide variety of orientations, as may be required for different missions.

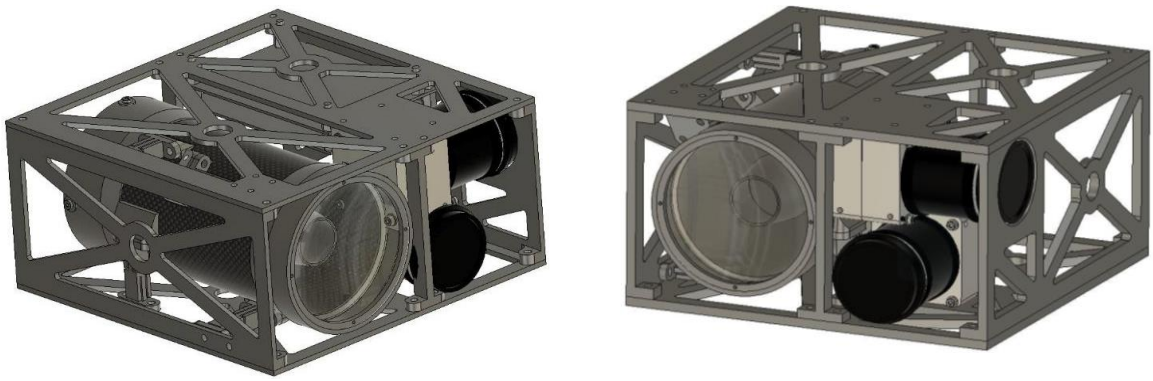

Figure 1. Two perspectives of the proposed IONEA deep space visual navigation instrument.

2 HARDWARE DESIGN

As mentioned in the previous section, three different visual sensors of two different types (two miniaturized star trackers and a high resolution optical navigation camera) are assumed to provide imaging data, while an image processing unit acquires and processes the images to extract measurements driving a visual navigation filter. Prototypes for each of the visual sensors have already been built at our offices, and will be further developed beyond TRL5 in the scope of two different Industrial R&D contracts. We have sought to establish a common miniaturized camera body for the proposed star trackers, such that both sensors and optical systems can be easily exchanged to build miniaturized hyperspectral or thermal infrared cameras for nanosatellite missions. As of today we are performing qualification for a hyperspectral camera based on this design, which we expect to demonstrate in orbit during the first half of 2023 as part of the AEROS satellite.

2.1 Star Tracker

The star tracker weighs about 450g and includes a modified COTS lens (to handle high thermal variations and vacuum conditions). Its' structure was designed in aluminium 7075-T6, black anodized to reduce stray-light. The camera has a diagonal field-of-view of about 18.2deg and is capable of acquiring images with 2048 x 2048 pixels at a rate of up to 10Hz and is capable of identifying objects (stars as well as planetary and small bodies) with an apparent magnitude of up to 6.5 with an exposure time of 50ms (it is also capable of detecting objects up to magnitude 10 for longer exposures and using image stacking).

Based on commonly used star pattern recognition algorithms and high-accuracy quaternion estimation methods (detailed in section 2.2) it is able to reach an accuracy of about 3arc-seconds RMS in the image plane. It also measures well under 0.5U, and consumes about 2W. The camera is connected to the image processing unit through a high-speed flat cable, which then provides crucial navigation data to an on board computer via CAN or SpaceWire interaces. The star tracker is meant to provide high-accuracy attitude estimates along with positioning measurements (for a full 3D positioning it needs to observe bodies along directions significantly separated between each other). For some applications (e.g. orbit determination while in a planetary orbit, or when orbiting a small body) star trackers may be better suited than the optical navigation camera, given the onboard memory implications of using a NAC for crater identification or terrain matching purposes.

For a descent and landing mission, these smaller cameras can also provide high enough horizontal positioning accuracy (1m at 6km altitude) to obviate the need for a higher resolution camera. On the other hand, accurate positioning in deep space is best achieved in practice using the optical navigation camera. The main star tracker camera specifications are described in Table 1.

Table 1. Specifications for the ST1 Star Tracker and Optical Navigation Camera.

Parameter	ST1 Star Tracker	Optical Navigation Camera
Optics	50mm, f/1.4	80mm, f/12
FOV	18.2 degrees	2.05 degrees
Dimensions	70.8 x 50 x 50 mm3	234 x 95 x 95 mm^3
Mass	450g	1Kg
Power	2W (max.)	3W (max.)
Temp	-30/60 (operational) -40/70 (non-operational)	-30/60 (operational) -40/70 (non-operational)
Voltage	6-17VDC	6-17VDC
Resolution	4MP (2048 x 2048 pixels)	12MP (4096 x 3072 pixels)
Pixel size	5.5 x 5.5µm2	5.5 x 5.5μm^2

Update rate	2Hz (nominal) 10Hz (max)	1Hz
Accuracy/IFOV	3 arc-sec RMS (image plane)	1.85 arc-sec (~4m@500km)
Stray Light	30°	30°
TRL	6 (current) 7 (Q3/2022) 9 (Q1/2023)	5

2.2 Optical Navigation Camera

The deep space Optical Navigation Camera (ONC), on the other hand (specifications are described in Table 1), is a Narrow Angle Camera weighing just short of 1kg. The camera is designed around a Cassegrain configuration with an f-number of 12. The optical system is kept in place by a stiff carbon fiber structure, which is both very light and highly stable (mechanically and thermally).

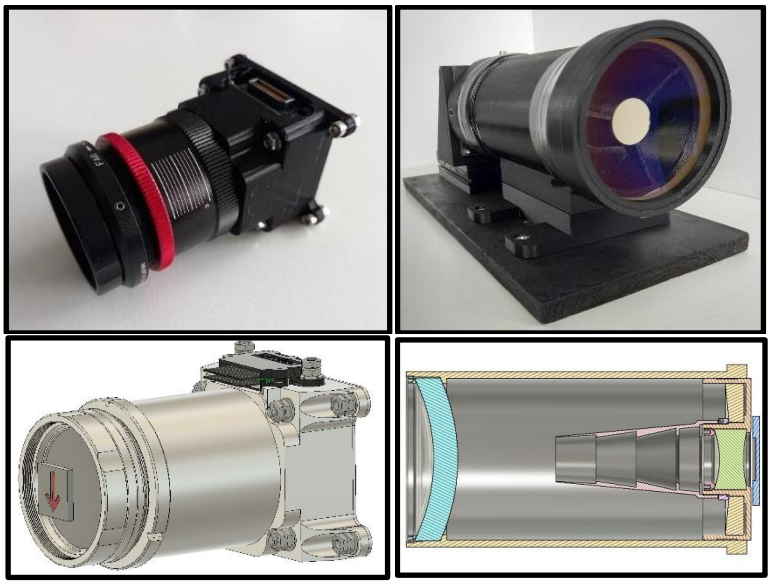

Figure 2. Prototypes and conceptual design for the Star Tracker and the Optical Navigation Camera.

The camera measures about 2U and the selected 12Mpixel sensor can capture images 2deg across with a resolution of 4096 x 3072 pixels - meaning that each pixel corresponds to about 1 300km at a range of 1 AU (highly useful for positioning in deep space). The camera uses a similar electrical and data interface as the star tracker, and is meant to be able to image distant objects with apparent magnitudes up to 9 (with long exposures), including planetary bodies and (the closest) small bodies to a spacecraft during an interplanetary transfer. In order to obtain 3D positioning data, image sets captured by the ONC must typically include objects very widely apart, which implies periodic spacecraft slews (the frequency of which depends on the pre-defined tracking error bounds established along a nominal transfer trajectory).

In the context of the Time Delay and Integration algorithm described in section 3.1.2, a hyperspectral camera has been developed within the same camera body as the star tracker, where an hyperspectral imaging sensor from IMEC (CMV2K LS150 VIS-NIR) based on a CMOSIS CMV2000 was used with hyperspectral filters on the visible and near infrared light spectrum.

The filters are disposed in a wedged pattern and distributed over two separated areas (empty interface zone with 120 lines). The VIS region is composed by 64 filters in the range 470-600nm and the NIR area by 128 filters that capture light in the 600-900nm range.

Finally, the processing unit is contained in a small 0.3U box between the star trackers and the optical navigation camera. It ensures that all cameras are simultaneously available at any given time to provide continuous attitude estimations and to enable precise ONC observations, contains all pertinent ephemerides and a priori map data for comparison, runs where most of the camera configuration and control software is locate, and runs the customized image processing algorithms and relative navigation and guidance algorithms as appropriate for each mission.

0	VIS
1	VIS
	...
62	VIS
63	VIS
empty interface zone	
64	NIR
65	NIR
...	
190	NIR
191	NIR

Figure 3. Hyperspectral Sensor Layout and sensor board.

For specific missions such as those involving descent and landing we have also developed navigation algorithms taking altimeter and IMU measurements as inputs, in addition to visual measurements, in order to provide accurate positioning from high altitude until as late in a mission as surface dust allows.

Table 2. Specifications for the Image Processing Unit.

Parameter	Value
Dimensions	130 x 106 x 30 mm^3
Mass	500g
Power	10W (max.)
SoC	Xilinx US+ ZU4EV
CPU	Quad Core ARM A53 @1.5GHz + Dual-Core ARM R5F @600MHz
FPGA	Xilinx UltraScale+
External I/F	SpW (TM/TC+image transfer)
Temp	-30/60 (operational) -40/70 (non-operational)
Voltage	6-17VDC
TRL	5

3 SOFTWARE DESIGN

The image processing unit is where most of the key software runs. It is derived from a high-performance payload data processor developed for micro-UAV multi-sensor applications and which is based on a Zynq Ultrascale+ SoC. Both this processing unit and each of the cameras developed at Spin.Works (including the star trackers and optical navigation camera described here) use the same

electrical and data connectors, something which greatly simplifies camera integration. A highly configurable IP core (SpinIP) has also been developed to ensure that sensor configuration and control and image acquisition is made easy for the entire family of sensors used at the company.

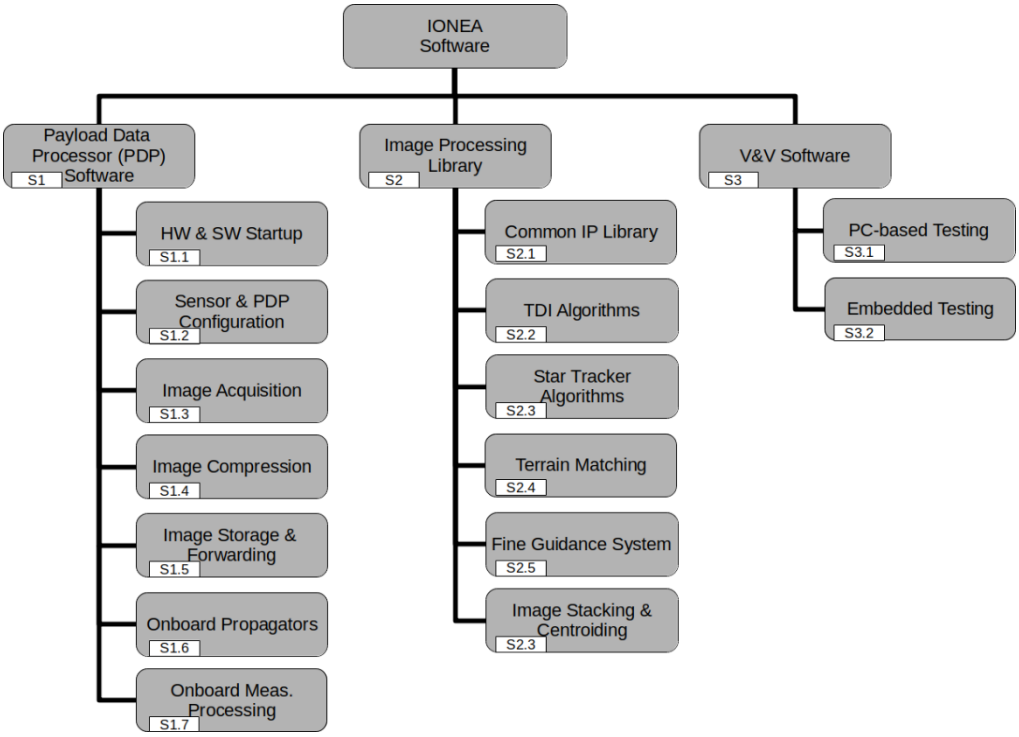

Figure 4. Software product tree for the IONEA instrument.

Beyond camera configuration and control and image acquisition, compression and storage algorithms, we have implemented onboard propagator and navigation software that accumulates measurements over long time periods to produce highly accurate positioning estimates. Navigation projections are made using observations which result from a number of different image processing algorithms that can be used at different mission times and phases. The algorithms include time-delay-integration algorithms, star tracker algorithms, terrain matching algorithms, or image stacking & centroiding algorithms. A software version of these algorithms was implemented as part of the development process in order to determine their individual performance during Monte Carlo simulations under tightly controlled conditions (the performance models were then fed to a covariance analysis tool in the context of representative scenarios, as will be seen in section 5.2). Then these algorithms were analysed in order to identify components which could be easily hardware-accelerated using the onboard FPGA with the support of High-Level Synthesis tools.

At the present time, results have been obtained for two particular algorithms using real imagery: the star tracker algorithms and the time-delay-integration algorithm (in the context of reconstruction of hyperspectral data using a push-broom camera). These are further described in the next section.

In addition, hardware-accelerated visual navigation tasks have been demonstrated using the same processor in the scope of the ESA AVERT project ([6], which involved extensive flight testing of terrain-relative navigation and hazard detection and avoidance algorithms) at a high enough rate (8-10Hz) to make feature tracking useful in a lunar or planetary landing scenario. Current work in the scope of the National R&D activity IONEA is aimed at significantly improving the prior functions such as to allow simultaneous multi-camera processing for future missions, while further laboratory, field and in-orbit demonstrations of the critical functions required for descent and landing are targeted for the near-future

3.1 Image Processing Algorithms

3.1.1 Star Tracker

In a brief summary, the Star Tracker algorithm can be decomposed into four main sub-routines which are described in the next few paragraphs:

- Image Processing
- Star Centroid Estimation and Pattern Identification
- Attitude Estimation

Pre-processing and preparation must be handled beforehand. Star tracker algorithms rely on star catalogues, which need to be adapted to every different algorithm and setup, containing reference attitude measurements for both star identification and attitude estimation stages.

The On-board Star Catalogue generation procedure is performed a priori and consists of pre-computing important data from the initial catalogue. The chosen star catalogue is the Bright Stars Catalogue [7], consisting of the 9096 brightest stars observed from Earth.

The accurate operation of the Star Tracker is highly dependent on the star distribution in the sky. The first step is to define the minimum relative star magnitude value, given the exposure time, camera sensor and appropriate minimum sky coverage (at least 95%), and filter out stars with brightness magnitudes bigger than that value. As a second step for the on-board catalogue, it is necessary to filter out stars that are too closely positioned to each other in order to eliminate misidentification cases where there would be expected two undistinguishable stars in the same pixel. The third and main objective of this preparation stage is to determine which stars can be considered neighbours, according to the camera projection model, namely lens field of view, detector size and focal length. The last stage of the pre-processing is to pre-allocate variables storing vital data for the subsequent star tracker subroutines, namely star identification and attitude estimation.

3.1.1.1 Image Processing

Given the acquisition rate, star trackers are subject to low exposure times. When capturing the dark sky with low exposure, star blobs get too dim to distinguish from the background, therefore it is necessary to enhance and process the raw captured frame to increase the robustness and accuracy of the subsequent stages.

The image processing procedure begins by filtering the opto-electrical noise at an early stage by smoothing out the star image using a gaussian kernel. Afterwards, the cleansed image is subject to a segmentation phase. Given a Signal-to-Noise ratio (SNR) study, it is possible to define a bottom floor value above which that SNR is ensured in order to obtain the potential star blobs and their position on the image plane, resulting in a binary mask.

A single-pass connected components stage [8] labels the different blobs and infers about both blob centre and blob area for each and every blob on the binary mask. The following figure depicts the basic connected components algorithm. Blobs of neighbouring pixels will be labelled with the same index (represented by a colour in the image) and this index will be incremented as the algorithm finds new blobs. The result is a sparse matrix where each blob (with index 1,2,3,4,...) is represented by a group of doublets (i,j), each doublet representing a pixel location on the image belonging to the blob.

Star blobs are modelled after an airy disk-shaped object which can therefore be roughly approximated to a gaussian shape. Bigger blobs define brighter stars. By filtering lower area blobs, we are increasing the SNR and increasing the chance of picking true positive stars. The following figure depicts the binary mask with red circles around blobs with valid area:

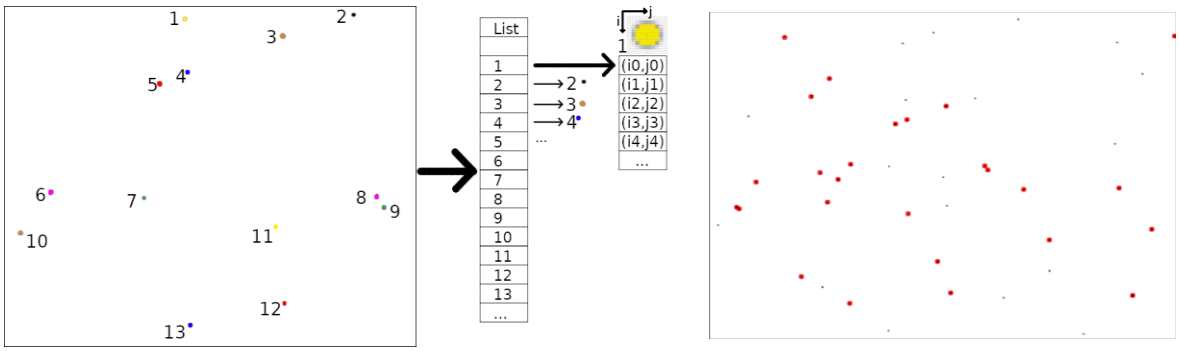

Figure 5. Connected Components Analysis (left) and Post-Processed Image (right). Red Blobs depict valid potential star blobs.

3.1.1.2 Star Centroid Estimation and Pattern Identification

It is necessary to perform a centroid refinement from the connected components estimate in order to increase the measurements accuracy. One of the most widely used, yet effective, centroiding methods is a 2D gaussian fitting procedure which is the chosen procedure for our star tracker centroid estimation stage, namely the Fast Gaussian Fitting [9]. The Star Identification process is highly influenced by (and thus vulnerable to) the star catalogue precision and centroid estimation. The present star identification procedure is built upon the Multi-Poles Algorithm [10], a highly promising star identification method that not only provides a fast star catalogue searching but also some effective proofing layers against false objects or even highly corrupted environments.

3.1.1.3 Attitude Estimation

Attitude estimation closes the gap between the reference coordinate vectors and the measured direction vectors based on image centroids. Two well-known methods achieve the global optima for the orthogonal matrix that minimises the Wahba's cost function. Though these methods guarantee a global convergence, their computational burden prevents their use in real applications. One of the most common methods is the QUaternion ESTimation Method (QUEST) [11] that uses a Newton-Raphson two-step iteration to easily converge towards a good estimation for the pose values therefore it is the chosen method.

3.1.1.4 Implementation Design

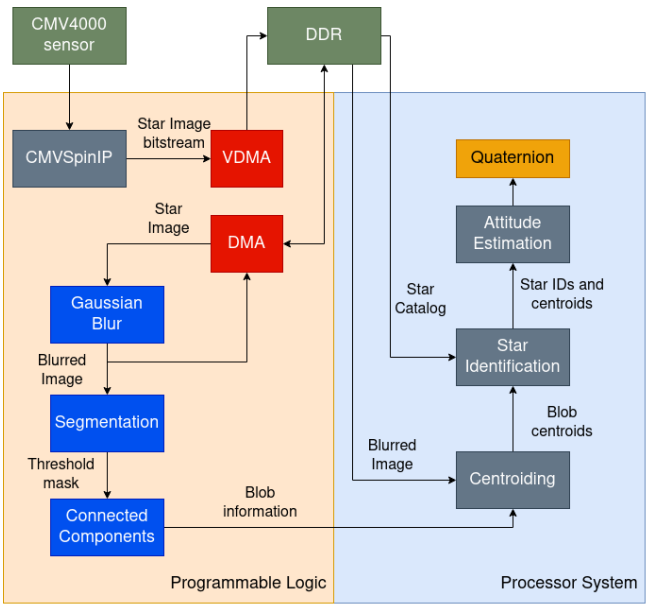

Figure 6. Star Tracker Image Processing Workflow

The image processing algorithms were accelerated using FPGA. They generally benefit from FPGA parallelization and dataflow. The following functions were subject to hardware implementation using high level synthesis tools: Gaussian Blur, Segmentation and Connected Components. The posterior operations, given their sequential nature, were implemented in CPU. The diagram in Figure 6 features a high level overview of the implementation.

3.1.2 Time Delay Integration (TDI)

Within the IONEA project we also investigated the potential application of image processing to a push-broom camera (although this has been made for the particular case of a hyperspectral camera most of this algorithm would apply to panchromatic push-broom cameras, which are often used in the scope of planetary observation missions). This involves successive image acquisitions from the same earth surface covering all the spectral bands present along the lines of the hyperspectral sensor. The frame acquisition is in this case controlled according to linear velocity and pitch rate in order to cover another hyperspectral layer at every frame.

3.1.2.1 Jitter Correction

Jitter can be defined as image translation along both the vertical and horizontal direction caused by image plane rotation. For example, motor vibration coupled to an imaging system will cause a blurring or translation effect on the final image. The Jitter Correction Module starts by computing 1D Correlation between the front-running 5 rows of the sensor at iteration i and the subsequent 5 rows of the next band at iteration i-1. Considering a neglectable spectral response difference between successive band respondes, the same patch of terrain is compared at different timestamps and infer the horizontal translation between those views. The subpixel estimation is obtained by performing a quadratic interpolation at a small window around the correlation maximum. That horizontal shift is compensated by convolving with a Lanczos 1D kernel that performs image translation and interpolation simultaneously.

3.1.2.2 Space-to-Depth: Hyperspectral Cube Construction

The Hyperspectral Product Building procedure can be simply put as overlapping the same terrain patches with each successive spectral receiver. At every iteration, after jitter correction, the hypercube is incrementally built by adding another layer on top of the last one, paying special attention to the band-wise offset (the same terrain patch is iteratively captured along successive spectral regions, offset by 5 rows). The final Hyperspectral Data contains the resulting virtual 150 bands. We have developed a simulator for the complete image generation process which uses Copernicus imagery to synthesize a hyperspectral image. The results are shown below in Figure 8.

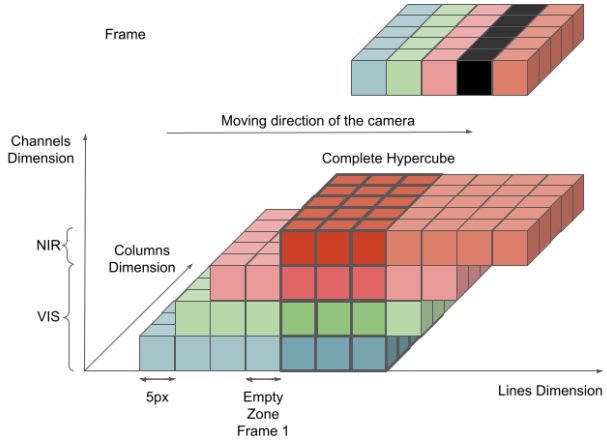

Figure 7. Hyperspectral Cube Building Diagram

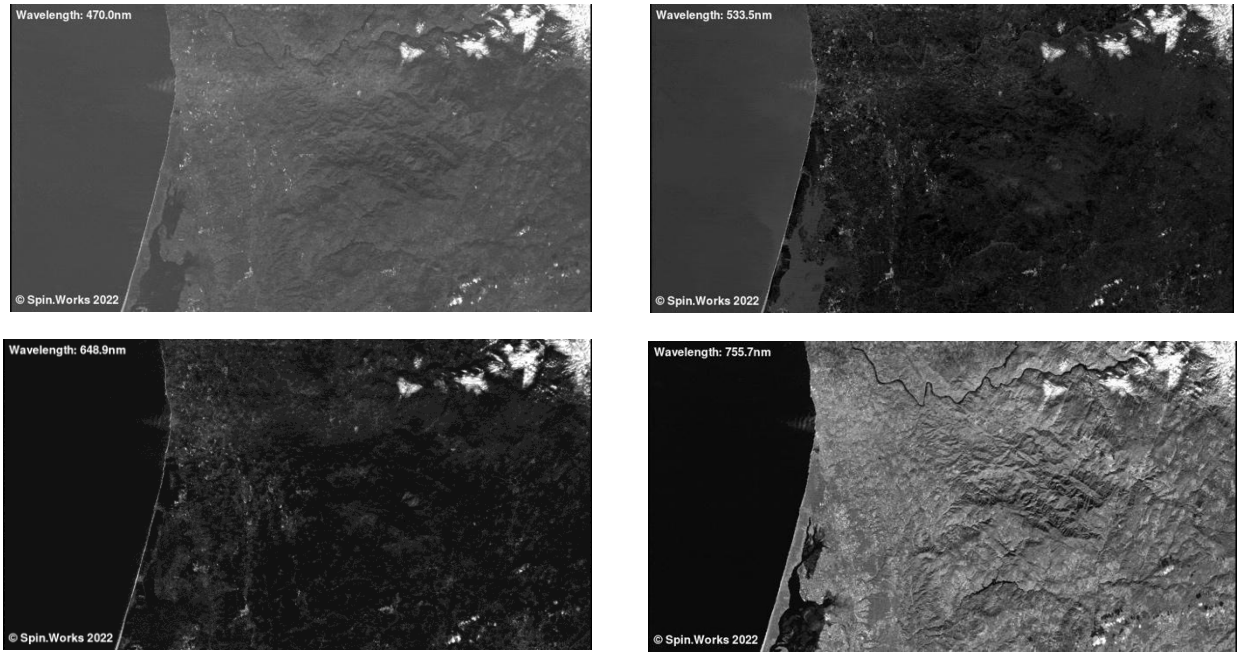

Figure 8: Hyperspectral Cube Results. Top left: 470 nm. Top right: 533.5 nm. Bottom left: 648.9 nm. Bottom right: 755.7 nm

3.1.2.3 Implementation Design

The high acquisition rate of the hyperspectral camera enforces the implementation to focus on a dataflow approach. This feature also allows an optimization of computing resources and diminished computing burden on the CPU side of action given the utilization of programmable logic. Finally, real-time on-board operation assures a higher compression rate, increasing the hyperspectral imagery downlink.

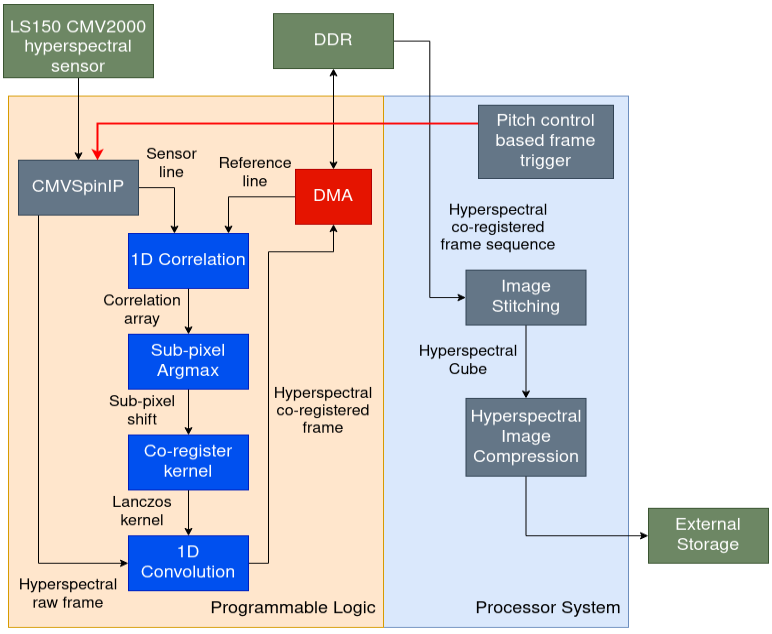

Figure 9. Hyperspectral Image Alignment and Hypercube image reconstruction process workflow.

4 TEST SETUP

As previously stated in section 2, Star Tracker and Optical Navigation Camera share similar electrical and data interface. In a testing environment, the developed IP core (SpinIP) enables the modularity necessary for a single platform, multiple sensor framework, resulting in a single testing platform shared by the two systems.

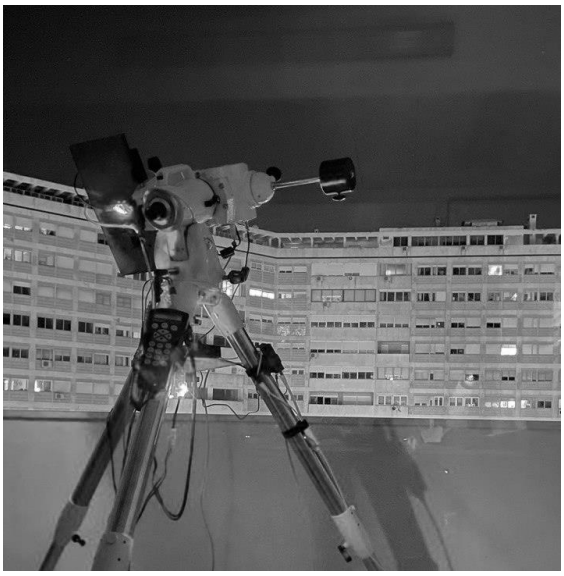

Figure 10. Star Tracker test platform.

The testing platform lays on a high-end commercial night sky observation gimbal (Figure 10), namely the Sky Watcher EQ6-R Pro [12], an equatorial mount capable of focusing any celestial object, for both star tracker and optical navigation camera, with an arcsec accuracy, a major advantage for star tracker validation. In summary, the gimbal is the mechanical actuator of the whole process.

While both cameras and systems share the same board type for their implementation, different enclosures were manufactured to accommodate the different acquisition optical systems. Figure 11 shows the different enclosures.

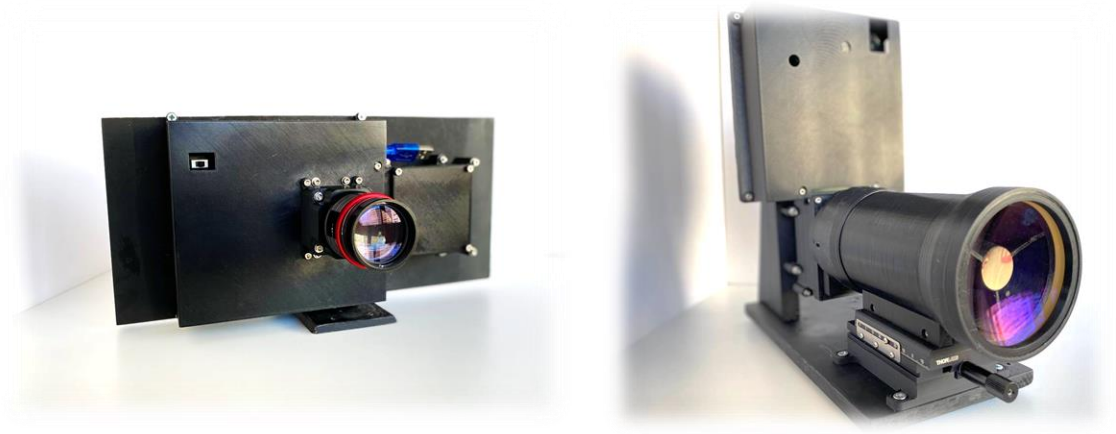

Figure 11. System Enclosures. Left: Star Tracker Mount. Right: Optical Navigation Camera Mount.

The common board setup within each enclosure, while differing in specific methods, allows real-time variable exposure time, ADC gain, PGA (programmable-gain amplifier) gain, black offset and voltage ramp values, which is of great interest for testing the algorithms on a wide range of operating conditions and study their impact on the overall robustness and SNR. This feature also enables a real statistical Monte Carlo analysis for both methods given the fast acquisition rates from gigabit ethernet TCP-IP streaming capabilities.

5 CASE STUDIES: MISSION SCENARIOS

5.1 Reference Trajectories

In order to study the potential of the proposed instrument for autonomous visual navigation, we have studied two particular scenarios where it could potentially be used: a small body mission and a lunar landing mission. For the first case, we have considered targeting the object 65803 Didymos, which is also the target for the ongoing NASA/ESA AIDA collaboration (of which DART, the NASA contribution, has already launched). For the second case, we separated a lunar landing mission in the GTO phase, two Lunar Transfer phases (an outgoing leg, followed by an incoming leg until Lunar orbit intersection – see Figure 13 –, then a lunar orbital phase, and a deorbit, descent and landing segment. The assumed vehicle is similar in size to the IAI Beresheet lunar lander [13] – about 180kg dry mass and ~600kg when fully loaded, and using a 400N engine with an Isp of 318s. The trajectories obtained are shown in Figure 12 and Figure 13.

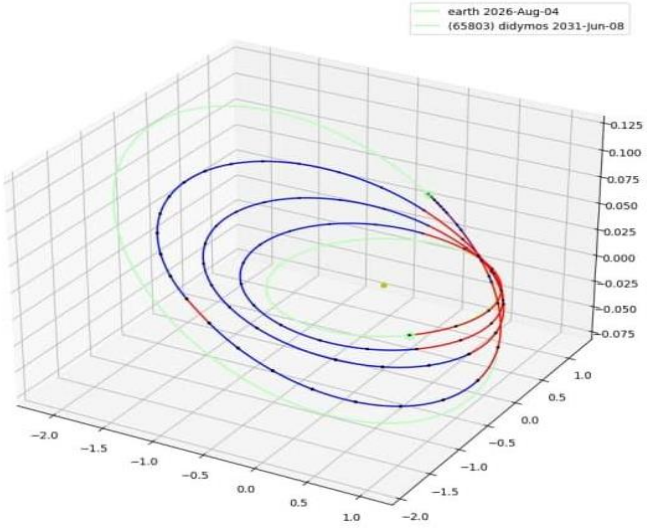

Figure 12. Optimal low-thrust transfer from the Earth-Sun L2 point to 65083 Didymos.

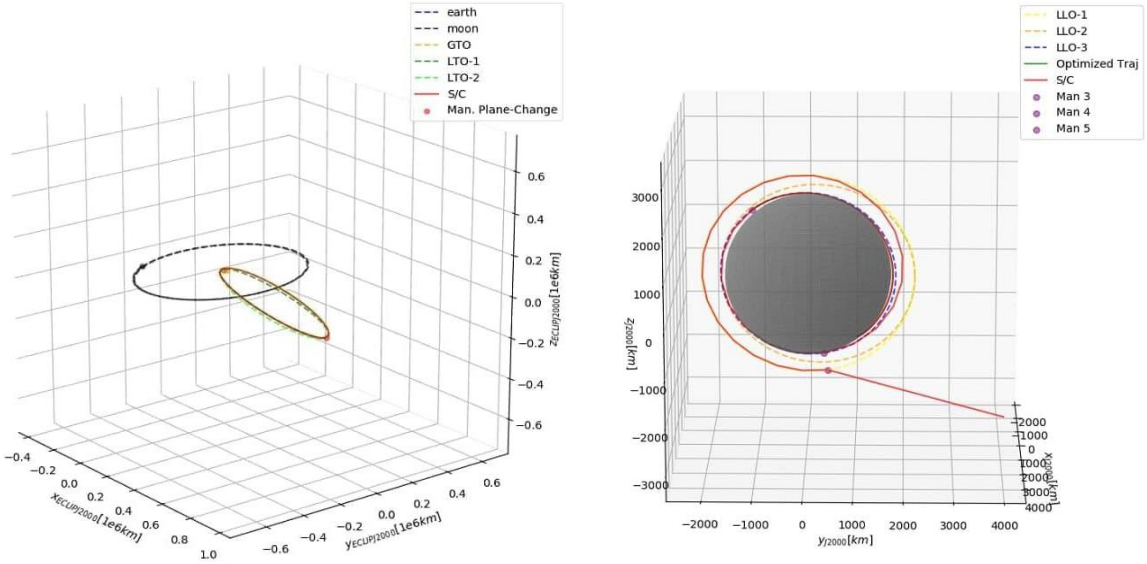

Figure 13. Lunar transfer strategy from GTO to Low Lunar Orbit (LLO): a) bielliptic transfer, b) lunar polar orbit insertion and orbital reduction until LLO.

5.2 Covariance Analysis Results

Following the definition of the reference trajectories for the two mission scenarios, we selected the measurements types: for small body mission we use centroiding on inner solar planets along with opportunistic observations of the brightest asteroids on the MPCORB database; whereas for the lunar landing case we used mostly centroiding and terrain matching, given the highly varying range relative to our target. The performance of each image processing algorithm is conservatively assumed to be no better than 1 pixel for either case. The positioning performance obtained for the small body and lunar landing missions, assuming the reference trajectory, camera design specifications and image processing algorithm performance is summarized in Figure 14 and Figure 15.
The analysis performed for the small body case, similar to that in [14] and described in more detail in [15] shows that autonomous vision-only navigation may be feasible for the interplanetary transfer phase of missions within the inner solar system. A knowledge of between 10-20000km prior to the approach phase (feasible with just two observations per month) results on a manageable approach phase where 1 observation per day is realized, leading to relative position knowledge of within 1km in the radial direction and about 10m in the remaining two axes just before arrival.

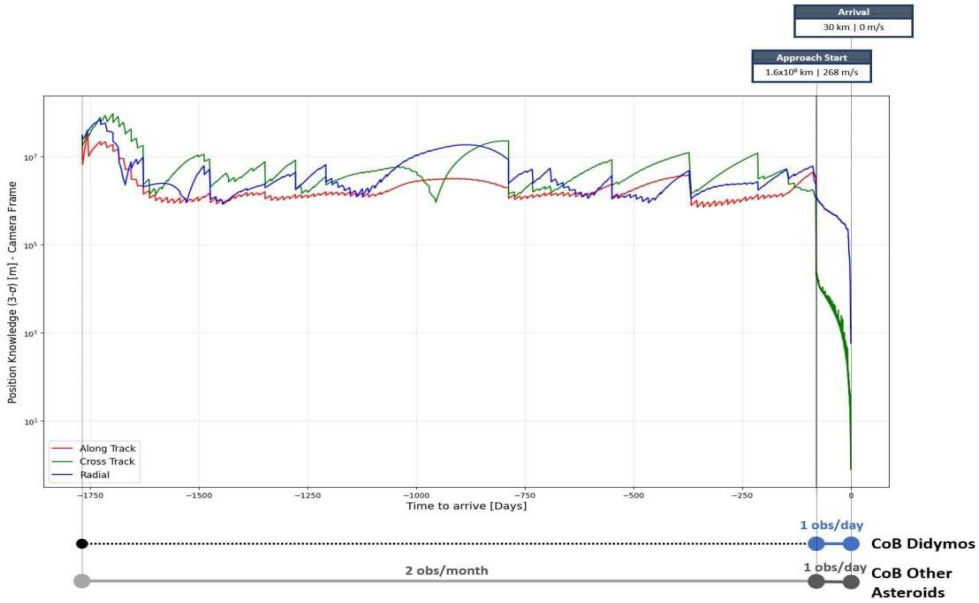

Figure 14. Vision-only position knowledge during a transfer to 65803 Didymos [15].

For the lunar landing case, and during both the outgoing and incoming legs of the bi-elliptic transfer, position knowledge is between 10-20km, and upon arrival in Lunar Orbit a few hours of observations are enough to reduce uncertainties to a few 100m and 0.1-0.2m/s. As the orbit is reduced to 100km, state knowledge stabilizes at around 0.1m/s and 100-200m, which is further improved to ~4cm/s and 30-60m once the final orbit is achieved (100 x 30km) prior to the descent and landing phase.

The results show that when using a system with the proposed specifications, it is possible to determine the position of a spacecraft to a very high accuracy using only visual measurements. This means that for both the small body and the lunar landing missions, knowledge can be bounded by frequent observations, and can be made to remain close to a safe level, thereby allowing a spacecraft to track a pre-defined trajectory within reasonable bounds. This suggests that it is feasible to autonomously steer a spacecraft from launch separation to low lunar orbit using only vision as the sole means of navigation.

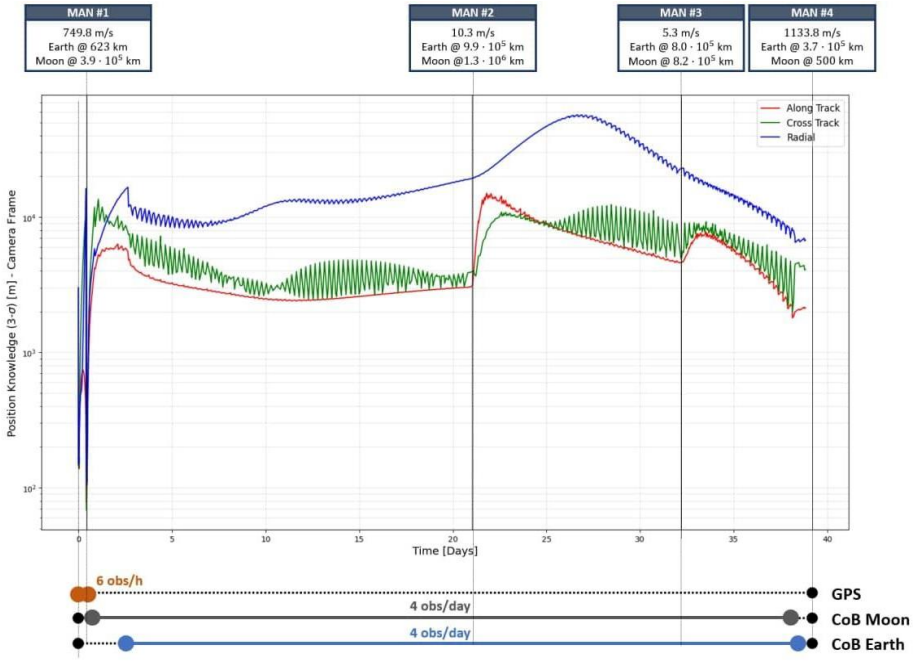

Figure 15. GNSS + vision-based position knowledge during bielliptic transfer for the lunar landing mission, using GNSS and Center-of-Brightness (CoB) data (from [15]).

6 CONCLUSIONS

Our primary intent with this activity is to present initial results, both analytical and practical, that raise a discussion on the feasibility of raising the level of autonomy for future deep space spacecraft by using autonomous optical navigation. Given the decreasing launch costs and the persistently high operational costs for interplanetary mission missions, we have sought to demonstrate that it is possible to acquire enough knowledge about a spacecraft position and velocity using only on board visual measurements, and that relative position knowledge in addition to precise attitude estimation (provided by star trackers) may well be enough to successfully carry out an end-to-end mission without ever relying on ground assets.

We have already built and characterized a prototype multi-sensor instrument that, once space-qualified, should enable fully autonomous navigation for a significant variety of applications, even beyond our present analysis of two representative cis-lunar and interplanetary missions. More work is still ahead, both at algorithm implementation as well as at integration level, in order to ensure that the total correction delta-V associated to this approach, albeit higher than for current missions, remains tolerable. At the moment we continue to focus on the space qualification of our cameras, with the intent of completing an in-orbit demonstrations by 2023. At that point we will perform a thorough in-flight characterization of real hardware, as well as a detailed performance assessment of the image processing algorithms as described here, that will become the basis for our next steps.

7 ACKNOWLEDGEMENTS

The work described in this paper was funded by the Norte 2020, Portugal 2020 and European Union through the European Regional Development Fund, under the contract NORTE-01-0247-FEDER-45192 (**IONEA – Visual Instrument for Space-based Observation and Autonomous Exploration)**.

8 REFERENCES

[1] Asmar S. and Matousek S., *Mars Cube One (MarCO) – Shifting the Paradigm in Relay Deep Space Operations*, SpaceOps 2016 Conference, 16-20 May 2016, Daejeon, South Korea.

[2] Capannolo A., Zanotti G., Lavagna M., Epifani E. M., Corte V. D., Zannoni M., Gai I., Pirrotta S. and Amoroso M., *Challenges in LICIA Cubesat Trajectory Design to Support DART Mission Science*, 70th International Astronautical Congress, Washington D.C., United States, 21-25 October 2019.

[3] Wahlund J.-E., Kohout T., Andrews D., Penttilä A. et. al., *Asteroid Prospection Explorer (APEX) Cubesat for the ESA Hera Mission*, EPSC-DPS Joint Meeting 2019, Geneva, Switzerland, 15-20 September 2019

[4] Goldberg H.R., Karatekin O., Ritter B., Herique A., Tortora P., Prioroc C., Gutierrez B.G., Martino P., Carnelli I., *The Juventas CubeSat in Support of ESA's Hera Mission to the Asteroid Didymos*, 33rd Annual AIAA/USU Conference on Small Satellites, Logan UT, United States,, August 3-8, 2019

[5] Jorgensen P.S., Jorgensen J.L., Denver T., *MicroASC – A Miniature Star Tracker*, Proceedings of The 4S Symposium: Small Satellites, Systems and Services (ESA SP-571). 20-24 September 2004, La Rochelle, France

[6] Câmara F., Oliveira J., Canilho J., Rodrigues M., Posse C., Dubois-Matra O., Alves J., *Real-time Implementation of the Hybrid Camera-Lidar Hazard Detection and Avoidance Software in Space-Qualified Hardware*, 10th International ESA Conference on Guidance, Navigation and Control Systems, Salzburg, Austria, 29 May – 2 June 2017.

[7] Hoffleit, D. and Warren, Jr., W.H., 1991, *The Bright Star Catalog, 5th Revised Edition (Preliminary Version).*

[8] M. J. Klaiber, D. G. Bailey, Y. O. Baroud and S. Simon, *A Resource-Efficient Hardware Architecture for Connected Component Analysis*, in IEEE Transactions on Circuits and Systems for Video Technology, vol. 26, no. 7, pp. 1334-1349, July 2016, doi: 10.1109/TCSVT.2015.2450371.

[9] Wan, Xiaowei & Wang, Gangyi & Wei, Xinguo & Li, Jian & Zhang, Guangjun. (2018). *Star Centroiding Based on Fast Gaussian Fitting for Star Sensors*. Sensors. 18. 2836. 10.3390/s18092836.

[10] Schiattarella, Vincenzo & Spiller, Dario & Curti, Fabio. (2017). *A Novel Star Identification Technique Robust to High Presence of False Objects: the Multi-Poles Algorithm*. Advances in Space Research. 59. 10.1016/j.asr.2017.01.034.

[11] SHUSTER, M. D., *Approximate Algorithms for Fast Optimal Attitude Computation*, Paper No. 78-1249, Proceedings, AIAA Guidance and Control Conference, Palo Alto, California, August 1978, pp. 88–95.

[12] http://skywatcher.com/product/eq6r-pro/

[13] Shyldkrot H., Shmidt E., Geron D., Kronenfeld J., Loucks M., Carrico J., Policastri L. and Taylor J., *The first commercial lunar lander mission: Beresheet*, 2019 AAS/AIAA Astrodynamics Specialist Conference, Portland ME, August 11-15, 2019.

[14] Esteves D., Seabra J., Carreira L., Hormigo T., Câmara F., *Dispersion Analysis and Autonomous Image-based Navigation on a Small Body Approach*, 10th International ESA Conference on Guidance, Navigation and Control Systems, Salzburg, Austria, 29 May – 2 June 2017.

[15] Hormigo T., Esteves D., Santos A., Afonso G., Câmara F., *Autonomous interplanetary mission design in a continued high operational cost scenario*, 8th International Conference on Astrodynamics Tools and Techniques (ICATT), Sopot, Poland, June 2021